Hindawi
Advances in Civil Engineering
Volume 2023, Article ID 9275977, 18 pages
https://doi.org/10.1155/2023/9275977

Research Article

Large-Scale Construction Waste Mountain-Mounding Technology Based on the Project in Meibei Lake Scenic Area

Miao Kang,[1] Xiongbin Guo,[2] Shoufu Li,[1] Jincheng Fan,[1] Yufei Xu,[1] Weiye Gu,[1] and Teng Wang[1]

[1]*China Construction Third Engineering Bureau Group Co. Ltd., Xi'an, Shaanxi 710065, China*
[2]*Xi'an Engineering Investigation and Design Research Institute, China National Nonferrous Metals Industry Co. Ltd., Xi'an, Shaanxi 710054, China*

Correspondence should be addressed to Jincheng Fan; fanjincheng1314@163.com

Received 10 May 2023; Revised 11 October 2023; Accepted 24 October 2023; Published 17 November 2023

Academic Editor: Jianyong Han

Copyright © 2023 Miao Kang et al. This is an open access article distributed under the Creative Commons Attribution License, which permits unrestricted use, distribution, and reproduction in any medium, provided the original work is properly cited.

In the backdrop of China's rapid economic growth and urbanization, the surge in construction waste poses mounting disposal challenges. This study primarily focuses on in-depth research and exploration of construction waste recycling technologies. By repurposing towering heaps of construction debris into artificial landscapes, it achieves resource reutilization and waste reduction, bearing profound significance for environmental protection, and resource utilization. Taking the Xi'an Meibei Lake Scenic Area construction waste embankment project as a case study, experiments on the physical properties of soil-construction waste mixtures were conducted. A three-dimensional computational model of the site was established, and typical cross-sections were selected for the slope stability calculations and analysis. This was coupled with on-site measurements to validate the practicality and effectiveness of the technology. The successful execution of the project has demonstrated the reliability of this technology, offering significant potential for widespread application and serving as a crucial reference for the similar projects.

1. Introduction

The continuous development of urbanization in China, accompanied by a large amount of construction waste, has increased year by year, and the conventional treatment method for this waste accumulation mostly involves landfills, cannot achieve the reuse of construction waste, and occupies resources. Zhang et al. [1] pointed out that the reuse of construction waste cannot be achieved in a short period of time, and Geo-Studio software was used to analyze the stability of the pile and to study the engineering protection. Fu [2] investigated that in urban parks, mountain-mounding makes waste into treasure, which both dissipates construction waste and promotes the development of urban landscape.

In the process of mountain-mounding, various types of soil materials are often involved, and the mechanical properties of the mounded soil play a crucial role in the quality of the engineering after mounding. In 2023, Chen et al. [3] examines the impact of cementing agent concentration and curing age on the hydraulic–mechanical properties of solidified loess through the utilization of Microbially Induced Calcium Carbonate Precipitation (MICP), an emerging biotechnological approach, and concluded that MICP holds great potential as a method to enhance the mechanical performance and water stability of loess.

In the study of Liu et al. [4], a mountain plasticity discrimination procedure was prepared and applied by using the parametric design language (APDL) in ANSYS finite element software.

To minimize displacements and deformations, the application of steel-sheet piles and anchor cables is essential for reinforcing soil after mountain-mounding. Through the finite element method (FEM), Han et al. [5] discovered that this composite support system efficiently mitigates deformation and ensures effective waterproofing in areas where anchor cables are present.

Using three-dimensional finite element models, Han et al. [6] investigated the mechanical characteristics of both embedded and nonembedded retaining walls, and also

provided a predictive method for the mechanical behaviors of the expansion project.

Lei et al. [7] studied the graded loading construction process of construction waste mounding hill project, and pointed out that mounding prepressure is the most economical and reasonable treatment scheme. Ma et al. [8] proposed prevention and control measures to promote foundation stability, such as controlling the rate of landfill, and verified the stability analysis of the mountain by monitoring and measuring. Cang et al. [9] carried out mathematical analysis of the stability of muddy soil and studied foundation treatment during artificial piled hill in soft soil area. Wan et al. [10] used displacement inverse analysis to analyze the stability of construction waste landfills. Other scholars have conducted studies on design and construction [11] and environmental friendliness [12, 13].

Relevant statistics show that construction waste emissions in China account for 30%–40% of the total urban waste [14, 15]. Kang and Li [16] showed that Xi'an city can reach about 40%, which enhances the resource utilization rate of construction waste up to about 20%, compared to developed countries where the resource utilization rate of construction waste is up to 90% or more, there is an obvious gap in China, and under the promotion of national regulations and related policies continuously improved, the reuse of construction waste in recent years continuous development.

Since 2012, Xi'an City has issued several pieces of legislation to promote the management of construction waste and improve the resource utilization rate of construction waste in Xi'an City, including the second amendment to the Regulations on the Management of Construction Waste in Xi'an City in January 2021, the Measures for Pursuing Responsibility for the Management of Construction Waste in Xi'an City in 2015, and the Notice on the Implementation of Opinions on Strengthening the Resource Utilization of Construction Waste by the General Office of Xi'an Municipal People's Government in 2018.

Wang [17] analyzed the utilization of construction waste in Xi'an, Kang and Li [16] and Tang [18] studied the problems of construction waste disposal, Ma [19] and Zhang [20] studied the ways and methods of construction waste management, and although some scholars in Xi'an have analyzed the major initiative of construction waste reuse, there is a lack of examples and studies related to the stability analysis of local waste making hills in Xi'an.

Therefore, it is of great reference significance to conduct the consolidation settlement and corresponding stability analysis, from the physical and mechanical properties test analyses to a three-dimensional calculation model, starting from the construction site example of Ripple Lake in Xi'an City, combined with the actual on-site measurements and quantifications.

2. Project Overview

The Jingshan Mountain-mounding construction project of Meibei Lake scenic area (Figures 1 and 2) is located in northern Beitou Village on the west bank of the Flood River in Xi'an City. The maximum distance between the northern and southern points of the project is approximately 444 m, the maximum distance between the eastern and western points is approximately 505 m, and the maximum height of the mounding construction is approximately 30 m. The Jingshan Mountain-mounding construction project is located on the northwest shore of Meibei Lake scenic area, the west side is the location of Yichun Han Yuan, and the southeast side of the lake is surrounded by water. Jingshan Mountain comprises construction waste and loess mixed with layered rolling mounding construction materials. The foundation of the Jingshan Mountain-mounding project site comprises soil in addition to miscellaneous fill (local cultivated soil layer), the lower Quaternary Holocene floodplain loess-like soil, the Quaternary Upper Pleistocene residual ancient soil, alluvial powder clay, and sandy soil.

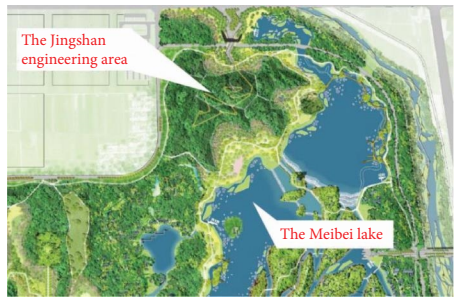

Figure 1: Diagram of the location of the construction work of the mounded body of Jingshan mountain.

Figure 2: Realistic photo of the Meibei Lake scenic area.

The West District Infrastructure Project Jingshan Heap Building represents a topographical transformation of site engineering (site engineering includes site preparation, vertical design, and protection engineering) into landscape engineering. The main structures on the mountain of Meibei Lake scenic are corridors, underpasses, trestle bridges, etc., which are sensitive to deformation and are large earth mountain-mounding projects.

The geomorphological pattern extends from south to north, encompassing river terraces, a loess plateau in front of the alluvial terraces, and loess plateaus. The microgeomorphology of the site is primarily influenced by three faults: the Weihe River North Bank Fault, the Yuxia-Tieluzi Fault, and the Qinling North Slope Pre-Mountain Fault. The proposed site's southern side is situated over 1 km away from the Yuxia-Tiehuzi fracture, thus its influence can be disregarded. No new active fractures have been detected within the proposed site or its surrounding area. The site is

Table 1: Main geotechnical physical and mechanical property indices.

Indicators	②-1 Layer of loess-like soil ($Q4^{al+pl}$)	②-2 Layer of loess-like soil ($Q4^{al+pl}$)	③-Layer of ancient soil ($Q3^{el}$)	④-Layer of powdered clay ($Q3^{al+pl}$)	⑤-Layer of powdered clay ($Q3^{al+pl}$)
Natural water content (%)	22.6	30.1	26.8	26.9	25.7
Natural gravity (km/m^3)	17.6	18.9	19.1	19.2	19.4
Compression coefficient (Mpa^{-1})	0.28	0.32	0.29	0.31	0.26
Cohesion (kPa)	31.0	17.9	24.0	23.0	25.6
Internal friction angle (°)	19.2	18.0	17.7	20.6	20.6

Table 2: Statistics of the percentage content of each particle group of the soil construction waste mixture.

Types of dam material	Percentage content of each grain group (%)					
	200–60 mm	60–40 mm	40–20 mm	20–10 mm	10–5 mm	< 5 mm
Soil mixture (before crushing)	13.47	1.22	6.62	2.16	12.92	63.61
Soil mixture (test)	/	1.41	7.65	2.49	14.93	73.52

Table 3: Controlled dry density and moisture content.

Type	Relative density		Compaction test				
	Minimum dry density ρ_{dmin} (g/cm^3)	Maximum dry density ρ_{dmax} (g/cm^3)	Maximum dry density ρ_{dmax} (g/cm^3)	Optimum water content (%)	Compaction	Test water content (%)	Test dry density ρ_d (g/cm^3)
Soil mixture (volume ratio 2 : 1)	1.29	1.61	1.71	14.7	0.93	12.4	1.59

positioned east of the Meibei Lake scenic area, approximately 60 m away. According to available information, there is no hydraulic connection between Meibei Lake, after undergoing impermeable treatment, and the groundwater level surrounding the site.

The stratum at the proposed site mainly consists of fill ①-1 layer of miscellaneous fill ($Q4^{ml}$), ①-2 layer of plain fill ($Q4^{ml}$), Quaternary Holocene alluvium, ②-1 layer of loess-like soil ($Q4^{al+pl}$), ②-2 layer of loess-like soil ($Q4^{al+pl}$), Quaternary Upper Pleistocene residual paleosol, ③-layer of paleosol ($Q3^{el}$), alluvial chalky clay, ④-layer of chalky clay ($Q3^{al+pl}$), and ⑤-layer of chalky clay ($Q3^{al+pl}$), etc. The main geotechnical indicators are presented in Table 1.

3. Simulation Results and Stability Analysis

3.1. Physical and Mechanical Properties of the Soil and Construction Waste Mixture

3.1.1. Particle Gradation Test and Analysis. Based on the actual laboratory analysis results, the construction waste (particle size > 60 mm) was crushed to make it uniformly distributed in each particle group below 60 mm, and the test results are shown in Table 2. The table indicates that the < 5-mm grain group is more than 63% of the actual soil construction waste mixture and over 73% of the test soil construction waste mixture, < 10-mm grain group accounts for over 76% of the actual soil construction waste mixture and over 88% of the tested soil construction waste mixture, and the > 60-mm grain group makes up 13.47% of the actual soil construction waste mixture.

3.1.2. Relative Density Experiment and Compaction Test Analysis. The fill mixture, with a soil volume to construction waste volume ratio of 2 : 1, contained sampled soil from the area designated by the construction party for soil collection and construction waste, which was taken from the building site that was being demolished and sent to the test laboratory. This was used to conduct particle analysis and gravity and moisture content tests according to the requirements of the fill mixture. On this basis, the maximum particle size of the test equipment was imposed upon the samples for compaction tests to determine the maximum dry density of the mixture and the optimal moisture content. According to 0.93 compaction to determine the controlled dry density and moisture content of the mixture, the test dry density of 1.59 g/cm^3 is shown in Table 3.

3.1.3. Consolidation Quick Shear Test. The stress-controlled EJ50-1A type coarse-grained soil large-scale straight shear test was conducted, and the experimental results are presented in Table 4.

3.1.4. Compression Test. The test was performed using a large consolidation instrument with a specimen diameter of 50.5 cm, and the sample was prepared based on the controlled dry density and moisture content of the test grade. According to the relevant test procedures and requirements, vertical loads were applied at 50, 100, 200, 400, and 600 kPa, and the vertical deformation was measured and recorded with a large range dial gauge. The e ~ P relationship curve is plotted in Figure 3 to determine the compression coefficients, compression moduli, and other parameters of the specimens.

Table 4: Direct shear test (consolidated quick shear).

Serial number	Material source	Water content (%)	Dry density of sample preparation ρ_d (g/cm^3)	Number	Cohesion (kPa)	Internal friction angle φ (°)
1	Soil mixture (volume ratio = 2 : 1)	12.4	1.59	Parallel ①	46	29.5
2				Parallel ②	44	29.3
3				Parallel ③	45	29.4
4				Parallel ④	42	29.3
5				Parallel ⑤	43	29.3
6				Parallel ⑥	45	29.5
7		10.5	1.54	Parallel ①	41	29.0
8				Parallel ②	40	28.9
9				Parallel ③	42	29.1
10				Parallel ④	44	29.2
11				Parallel ⑤	43	29.1
12				Parallel ⑥	42	29.0

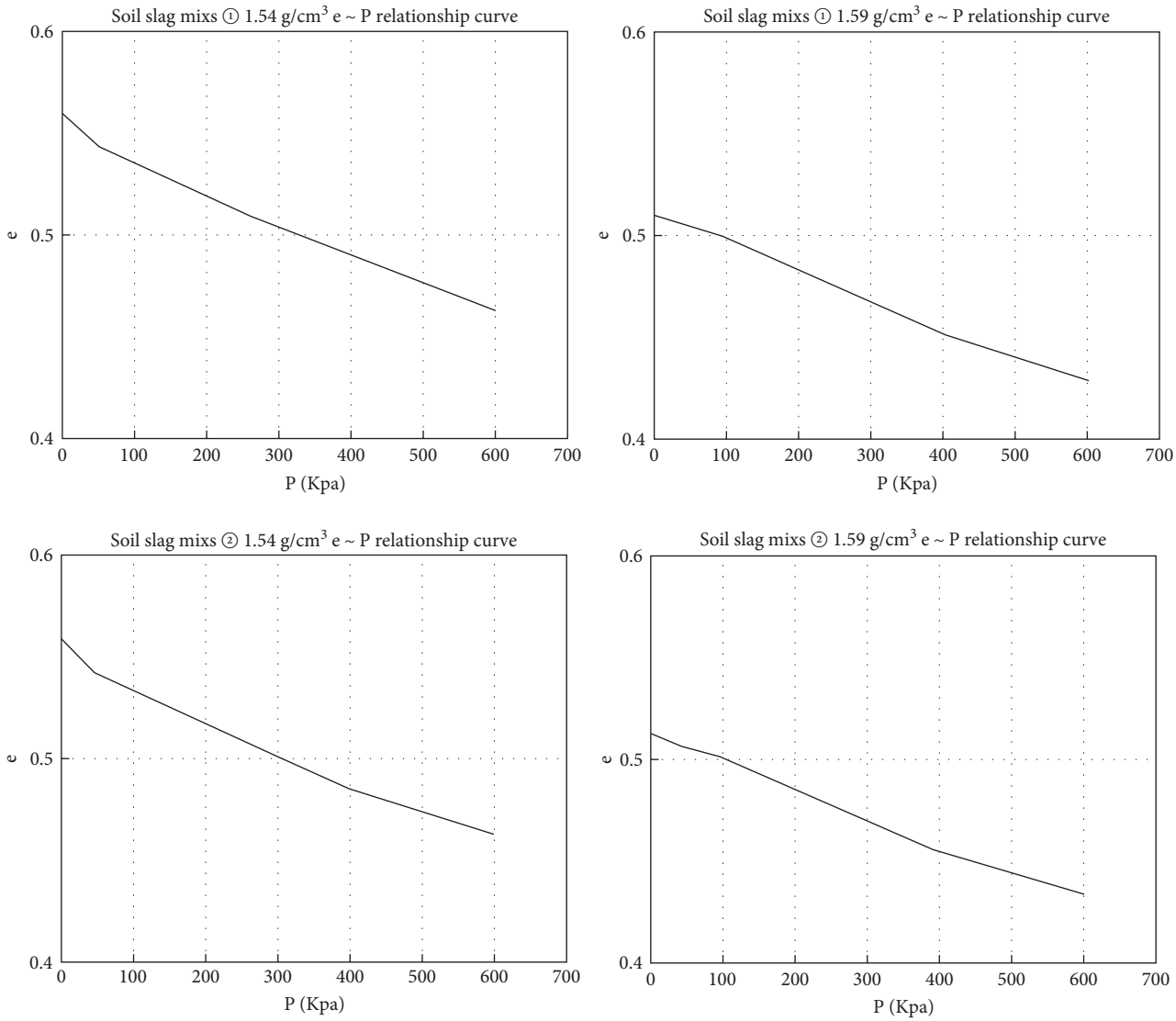

Figure 3: e ~ P relationship curves.

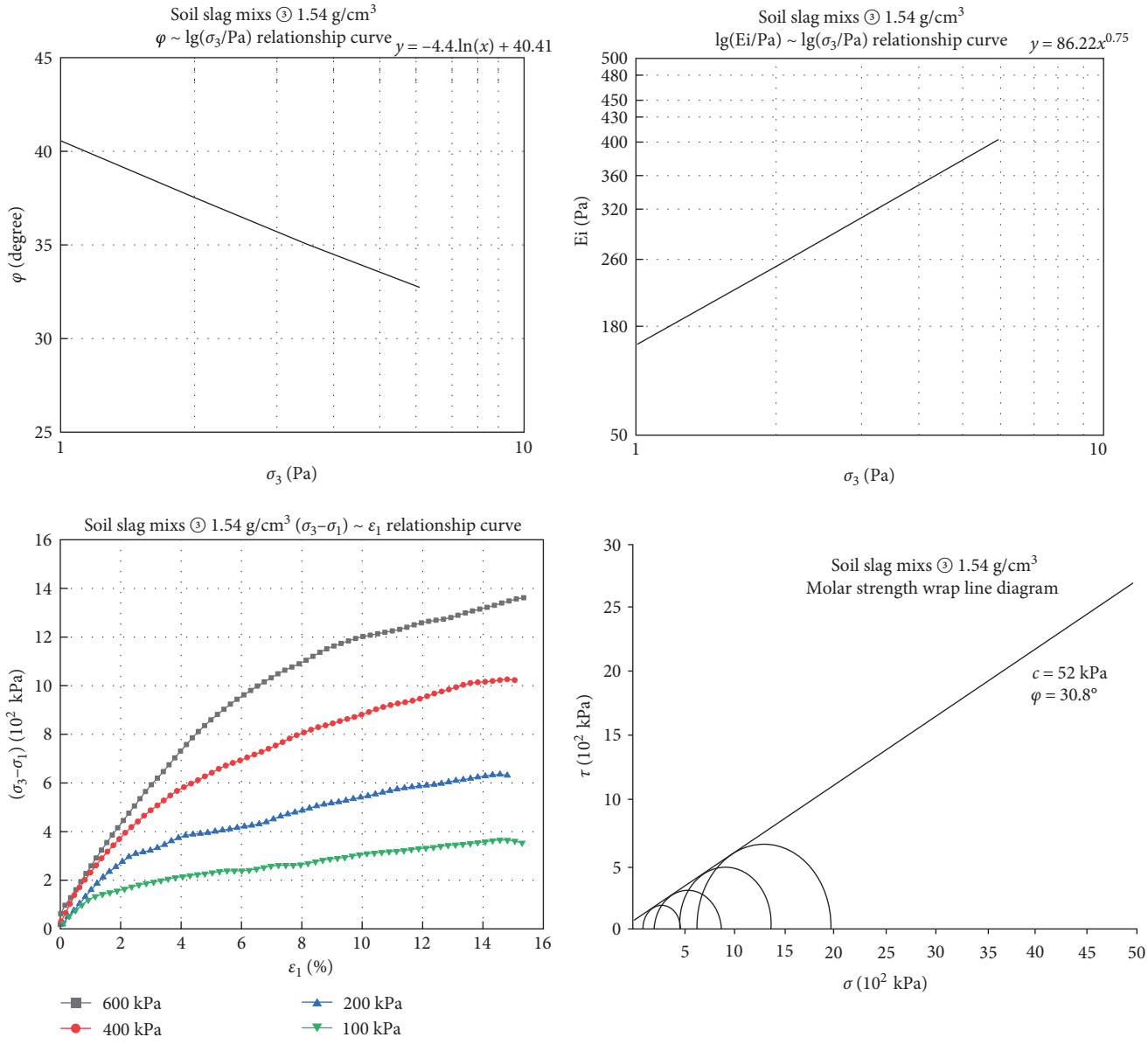

FIGURE 4: Triaxial test relationship curves.

From the compression curve and test results, it can be observed that with increasing vertical load, the vertical deformation increases while the pore ratio decreases. As the load increment is applied gradually, the soil compaction and particle crushing correlate, so the compression coefficient, compression modulus, and other deformation indices may not necessarily change monotonically. The test results reveal that the compression modulus of the soil and construction waste mixture falls within the range of 103–104 kPa, indicating a medium-compressibility material.

3.1.5. Static Triaxial Test. The static triaxial shear test was carried out using an SZ-2A triaxial shear instrument with a 300-mm specimen diameter for coarse-grained soils, and the samples were prepared to meet the controlled dry density and moisture content requirements as per the specified grading for the test. The Duncan model (E ~ B mode) and the linear and nonlinear shear strength indices were determined. The test followed the Geotechnical Test Procedure (SL237-199) with an inner diameter of 30 cm and a net height of 60.5 cm. The specimens were filled in three layers, and the shear rate was controlled at 2.0 mm/min. The stress–strain curves are depicted in Figure 4, and the corresponding test results are presented in Table 5.

The triaxial shear test results indicated that the stress–strain curves generally followed the assumption of a Duncan-Tension hyperbolic relationship before reaching the peak value. In this test, the molar circle strength envelope largely conforms to the linear law of the Cullen's strength criterion within the circumferential pressure range. This observation aligns with the patterns observed in the compression test results.

Table 5: Compression test results.

Duncan model parameters (E-B model) results table									
Serial number	Material source	Water content (%)	Dry density of sample preparation, ρ_d (g/cm^3)	Number	Duncan model parameters (E–B model)				
					K	n	R_f	φ_0 (°)	$\triangle\varphi$ (°)
1	Soil mixture	12.4	1.59	Parallel ①	136.9	0.55	0.73	42.5	10.5
2				Parallel ②	138.6	0.55	0.71	42.3	9.9
3				Parallel ③	139.4	0.53	0.71	42.6	10.6
Shear strength parameters results table									
Serial number	Material source	Water content (%)	Dry density of sample preparation, ρ_d (g/cm^3)	Number	Shear strength parameters				
					$\varphi = \varphi_0 - \Delta\varphi \lg(\sigma_3/p_a)$		$\tau = c + \sigma \tan\varphi$		
					φ_0 (°)	$\triangle\varphi$(°)	c (kPa)	φ (°)	
1	Soil mixture	12.4	1.59	Parallel ①	42.5	10.5	58	32.4	
2				Parallel ②	42.3	9.9	56	32.5	
3				Parallel ③	42.6	10.6	63	32.0	

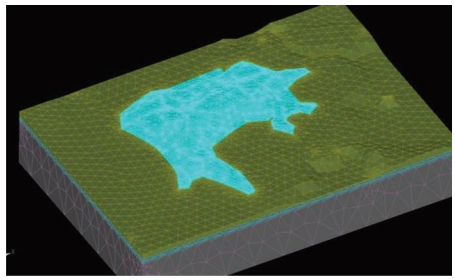

Figure 5: 3D finite element mesh computational model.

Considering that the maximum size of the actual coarse material at the site is larger than the maximum size of the test material, the test gradation involves artificially crushed construction waste and soil mixture, which may have certain implications. Therefore, it is crucial to enhance safety monitoring during construction and rely on real-time feedback analysis of monitoring data to predict and guide subsequent construction activities.

3.2. Jingshan Mountain Model Construction

3.2.1. Computational Model. A 3D (three-dimensional) finite element mesh computational model is established as shown in Figure 5.

3.2.2. Calculation of Working Conditions and Parameters. The consolidation settlement processes of the foundations were calculated for three loading rates assuming durations of 12 months, 18 months, and 24 months.

The mountain section is simulated using layer loading, with a total of twelve layers and a layer height of 2.5 m. The elevation of the foundation's bottom surface is set at 313.0 m, resulting in a foundation thickness of approximately 100 m. Calculation points for pore pressure observation and displacement observation are established. The selected calculation parameters for stress-deformation calculations are provided in Table 6, while the parameters for anti-slip stability calculations are given in Table 7.

3.3. Jingshan Mountain Consolidation Settlement Analysis

3.3.1. Calculation Principle. Biot consolidation theory is a comprehensive three-dimensional theory that accurately captures the interaction between pore pressure dissipation and soil skeleton deformation. It was initially formulated by Biot in 1941, based on a rigorous consolidation mechanism. In contrast, Terzaghi's consolidation theory, which is based on one-dimensional consolidation, lacks accuracy when applied to two- and three-dimensional cases. Biot's theory, on the other hand, provides a more rigorous and accurate representation of the interplay between pore pressure dissipation and soil skeleton deformation, commonly known as true three-dimensional consolidation theory. The theory is applicable to the consolidation of saturated soils.

A differential volume is assumed for the soil body. If the volume is considered only with respect to gravity, the z-coordinate is positive upward and the pressure is positive by pressure, then the three-dimensional equilibrium differential equation is as follows (Equation (1)):

$$\begin{aligned} &\frac{\partial \sigma_x}{\partial x} + \frac{\partial \tau_{xy}}{\partial y} + \frac{\partial \tau_{xz}}{\partial z} = 0 \ \frac{\partial \tau_{xy}}{\partial x} + \frac{\partial \sigma_y}{\partial y} + \frac{\partial \tau_{yz}}{\partial z} \\ &= 0 \ \frac{\partial \tau_{xz}}{\partial x} + \frac{\partial \tau_{yz}}{\partial y} + \frac{\partial \sigma_z}{\partial z} = -\gamma, \end{aligned} \tag{1}$$

where γ is the weight of the soil and the stress is the total stress acting on the soil.

According to the effective stress principle, the total stress is the sum of the effective stress and the pore pressure μ, and the pore water is not subject to shear stress, which is expressed by the matrix as follows (Equation (2)):

$$\{\sigma\} = \{\sigma'\} + \{M\}\mu. \tag{2}$$

Among them: $\{M\} = [11, 100]^T$

Table 6: Calculation parameters selected for the stress–deformation calculations.

Soil layer	R_f	K	n	D	G	F	Cohesion (kPa)	Internal friction angle (°)
②-2 Layers of loess-like soil	0.723	50.4	0.674	7.876	0.123	0.106	41	27.1
③-Layer of ancient soil	0.624	46.7	0.612	5.726	0.130	0.114	48	26.5
④-Layer of powdered clay	0.392	47.9	0.404	7.575	0.133	0.105	45	27.6
⑤-Layer of chalky clay	0.488	54.3	0.336	5.150	0.136	0.151	47	27.4

Table 7: Calculation parameters selected for the anti-slip stability calculations.

Material name	Weight capacity (KN/m^3)	Floating capacity (KN/m^3)	Cohesion (KPa)	Friction angle (°)	Cohesion (kPa) (underwater)	Friction angle (°) (underwater)
Soil mixture	17.1	8.0	31.5	20.4	30	18
Loess layer	17.6	8.6	18.0	16.0	16.0	14.0
Paleosol	19.1	10.2	28	18.5	26	16.5
Powdered clay	19.2	10.2	22	19.5	20	17.5

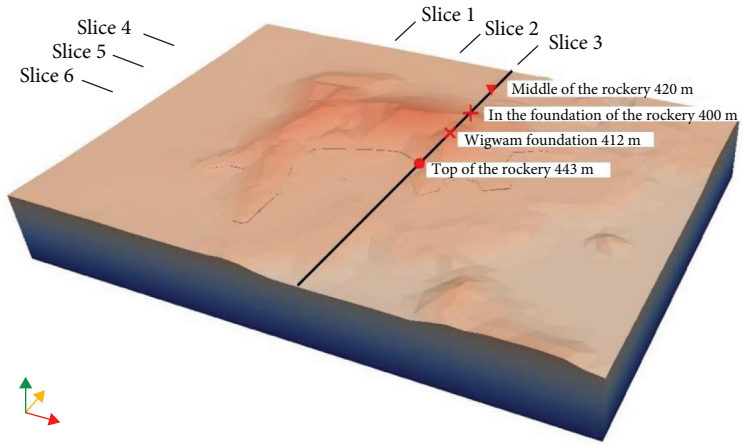

Figure 6: Slicing position.

that is (Equation (3)):

$$\frac{\partial \sigma_x^{'}}{\partial x}+\frac{\partial \tau_{xy}}{\partial y}+\frac{\partial \tau_{xz}}{\partial z}+\frac{\partial u}{\delta x}=0\ \frac{\partial \tau_{xy}}{\partial x}+\frac{\partial \sigma_y^{'}}{\partial y}+\frac{\partial \tau_{yz}}{\partial z}+\frac{\partial u}{\delta y}=0\ \frac{\partial \tau_{xz}}{\partial x}+\frac{\partial \tau_{yz}}{\partial y}+\frac{\partial \sigma_z^{'}}{\partial z}+\frac{\partial u}{\delta z}=-\gamma, \tag{3}$$

where $\frac{\partial u}{\delta x}$, $\frac{\partial u}{\delta y}$, and $\frac{\partial u}{\delta z}$ are the unit permeabilities in each direction. This equation is an equilibrium differential equation established with the soil skeleton as the detached body.

3.3.2. Calculation Results. For this model, a total of six slices were analyzed, and their respective locations can be seen in Figure 6. Vertical and horizontal slices were conducted for each slice location throughout the construction period. The settlement clouds for slices 1 through 6 are displayed in Figure 7, respectively.

Settlement calculations and analyses were carried out to assess the impact of different construction completion periods, specifically at 12 months, 18 months, and 24 months. The calculations focused on evaluating the settlement, horizontal displacement, and overburden pressure under varying working conditions. The results for Profile 3-3 are summarized in Table 8. Furthermore, Figure 7 provides a visual representation of the analyses and calculations for specific stages of the construction process.

Only the results of the settlement, horizontal displacement, and overhole pressure for a construction period of 24 months are listed below. The contour map of the settlement analysis is shown in Figure 8, the settlement development curve of the monitoring points is shown in Figure 9, the horizontal displacement development curve of the monitoring points is shown in Figure 10, and the overhole pressure development curve of the monitoring points is shown in Figure 11, and the superhole pressure development curves of the monitoring points in different construction periods are shown in Figure 12.

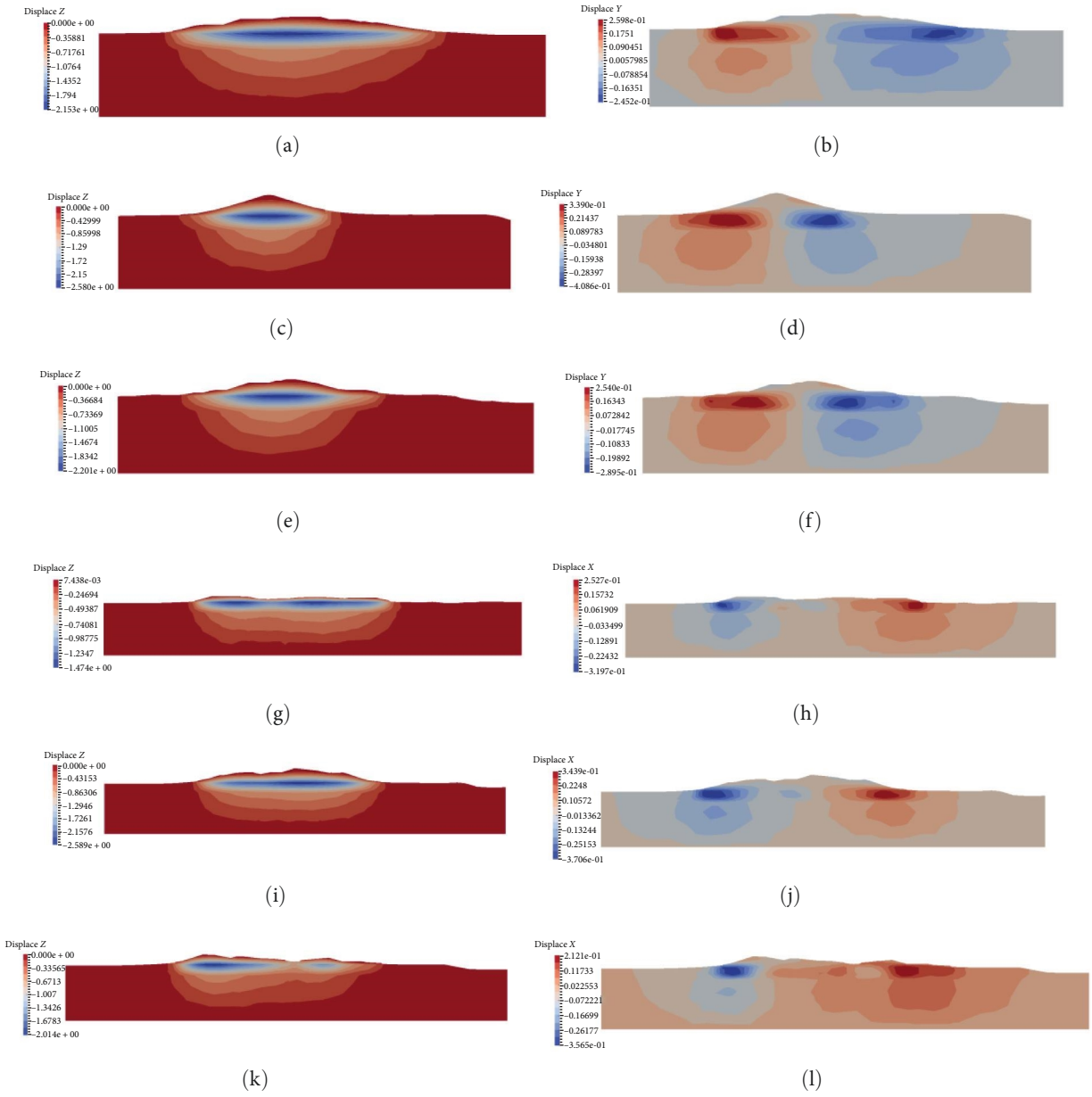

Figure 7: Finished construction period slices. (a) Settlement slice 1 during the completion period (unit: m). (b) Horizontal displacement slice 1 during the completion period (unit: m). (c) Settlement slice 2 during the completion period (unit: m). (d) Horizontal displacement slice 2 during the completion period (unit: m). (e) Settlement slice 3 during the completion period (unit: m). (f) Horizontal displacement slice 3 during the completion period (unit: m). (g) Settlement slice 4 during the completion period (unit: m). (h) Horizontal displacement slice 4 during the completion period (unit: m). (i) Settlement slice 5 during the completion period (unit: m). (j) Horizontal displacement slice 5 during the completion period (unit: m). (k) Settlement slice 6 during the completion period (unit: m). (l) Horizontal displacement slice 6 during the completion period (unit: m).

3.3.3. Analysis of the Results. In this paper, the stress-deformation of the Jingshan mountain-mounding project during the mounding process was analyzed by using Biot consolidation calculations, and the displacement development and pore pressure dissipation processes of the calculation model were obtained. The construction period of the rockery mounding in the calculation was simulated for 12 months, 18 months, and 24 months, extending until 24 months after the completion of construction. The main conclusions were obtained as follows:

(1) Construction activities generate superporous water pressure in the foundation, which gradually dissipates over time. The variation of maximum superporous pressure during the process is shown in Table 9, where the maximum superporous pressure generated in the foundation and the corresponding time of occurrence are summarized in Table 9.

Based on the ground investigation results, the project site exhibits soft plastic state ②-2 layer loess-like soil, the

Table 8: Summary of consolidation settlement calculations for Profile 3-3.

Profile 3-3	End of construction	12 Months after the end	24 Months after the end
Filling period of 12 months			
Maximum settlement (m)	2.12	2.48	2.64
Maximum horizontal displacement (m)	0.44	0.428	0.420
Maximum superporous pressure (kPa)	196.0	43.4	8.2
Degree of consolidation	0.678	0.876	0.960
Filling period of 18 months			
Maximum settlement (m)	2.25	2.58	2.65
Maximum horizontal displacement (m)	0.42	0.408	0.402
Maximum superporous pressure (kPa)	128	34.6	6.1
Degree of consolidation	0.768	0.931	0.978
Filling period of 24 months			
Maximum settlement (m)	2.41	2.64	2.68
Maximum horizontal displacement (m)	0.40	0.392	0.391
Maximum superporous pressure (kPa)	79.8	19.8	3.8
Degree of consolidation	0.798	0.912	0.985

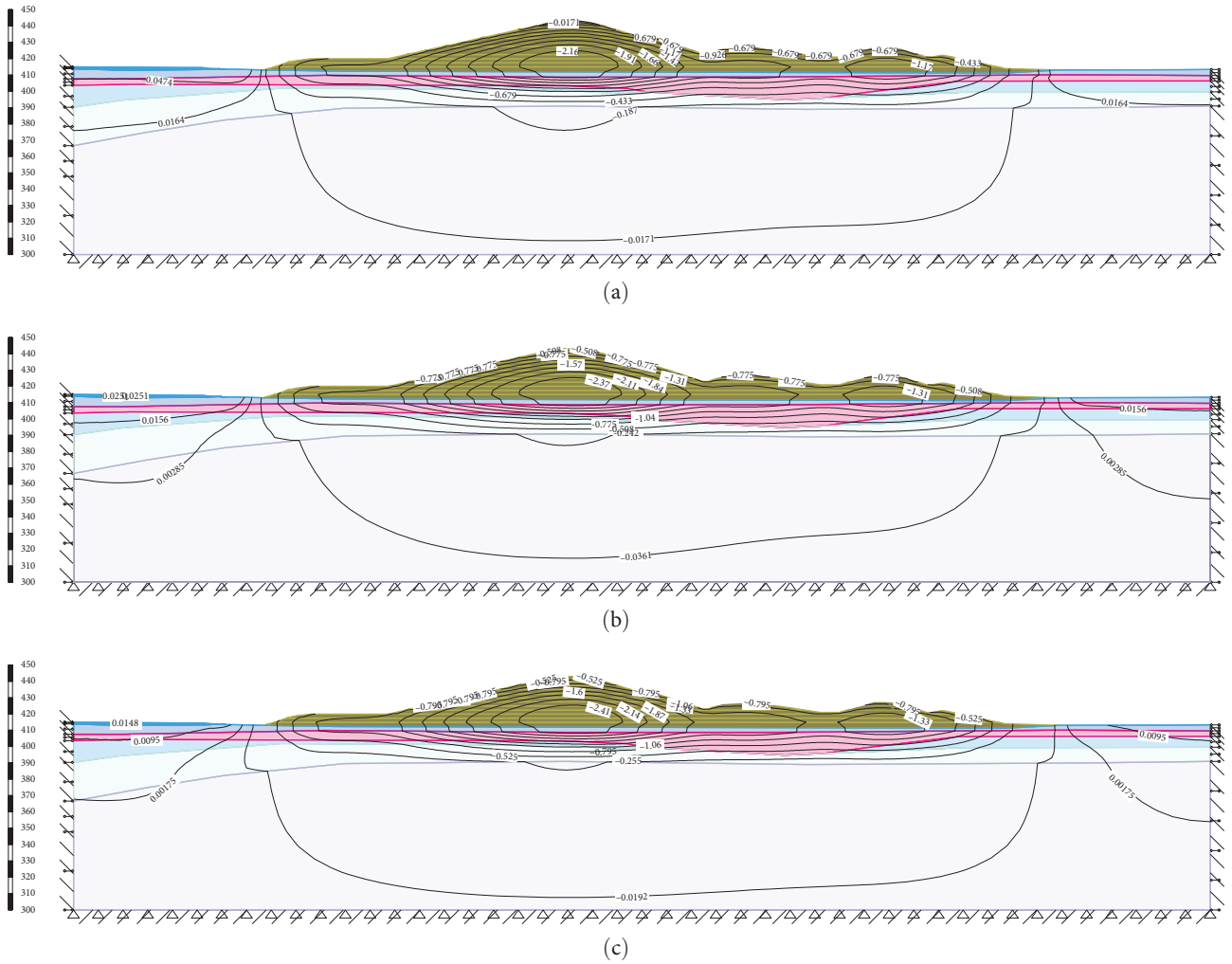

Figure 8: Settlement analysis contour map. (a) Settlement contour map at the end of construction (unit: m). (b) Settlement contour map 12 months after the end of construction (unit: m). (c) Settlement contour map for 24 months after the end of construction (unit: m).

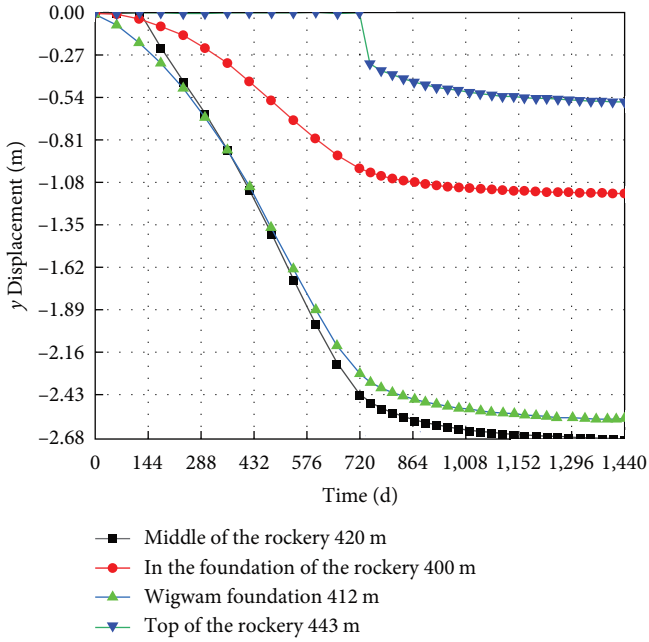

Figure 9: Settlement development curve of the monitoring points (24-months construction period).

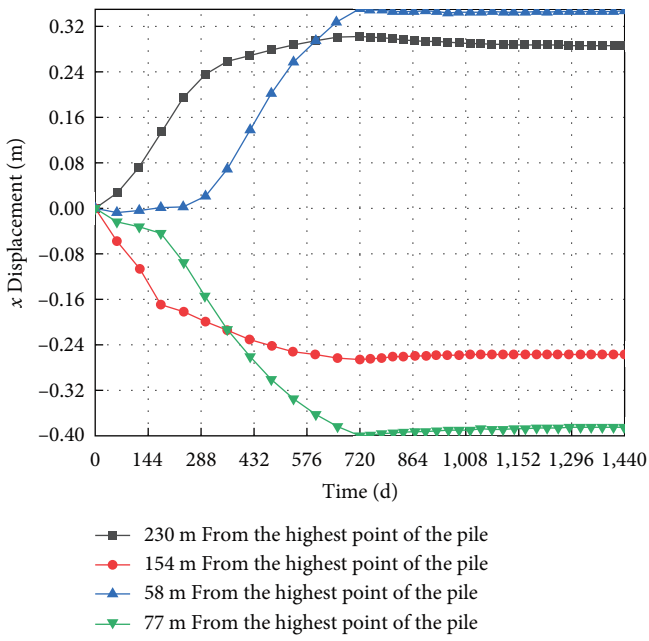

Figure 10: Horizontal displacement development curve of the monitoring points (24-months construction period).

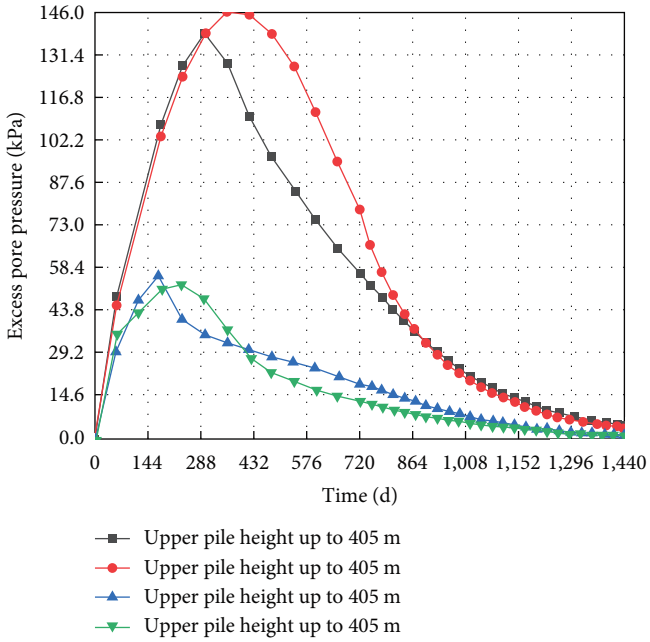

Figure 11: Overhole pressure development curve of the monitoring points (24-months construction period).

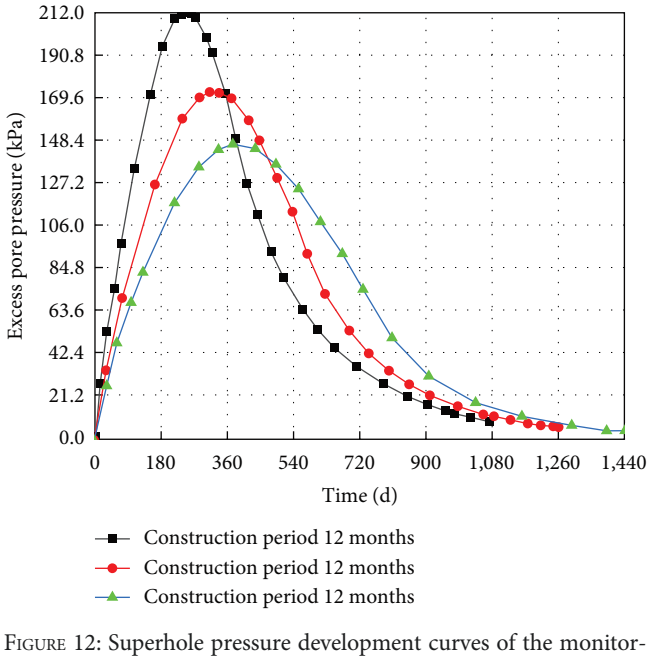

Figure 12: Superhole pressure development curves of the monitoring points in different construction periods.

thickness of most areas of the soil layer is 3.00–4.00 m, and the thickness only in the southwest part of the region (borehole number 30, 37, 38, 55, and 56) is 8.00–9.00 m. The mechanical properties of the foundation are poor, its permeability is weak, and the upper mound load caused by the superporous pressure does not easily dissipate. Calculations indicate that the construction-induced superporous pressure is affected by the upper mound load and the physical properties of the foundation, and the larger the upper mound load and the poorer the permeability of the foundation are, the larger the superporous pressure is, and the slower it dissipates. It is observed that approximately 24 months after the end of the construction period, the excess pore water pressure caused by mounding has largely dissipated.

(2) The settlement values of the project under the three working conditions are summarized in Table 10.

(3) The results of the horizontal displacement show that a certain amount of horizontal displacement is generated

Table 9: Summary of maximum superporous pressure and its occurrence.

Work conditions	Maximum overhole pressure during the whole process		Calculation of end overhole pressure (kPa)
	Maximum value (kPa)	Time of occurrence	
Construction period 12 months	211.9	$T = 240$ days, Mound height to elevation 432.5 m	8.2
Construction period 18 months	172.7	$T = 315$ days, Mound height to elevation 430.0 m	6.1
Construction period 24 months	146.3	$T = 360$ days, Mound height to elevation 427.5 m	3.8

Table 10: Summary of settlement values.

Work conditions	Settlement during construction (m)		Settlement during consolidation (m)		Total settlement during calculation (m)
	Value	Percentage (%)	Value	Percentage (%)	
Construction period 12 months	2.12	80.3	0.52	19.7	2.64
Construction period 18 months	2.25	84.9	0.40	15.1	2.65
Construction period 24 months	2.41	89.9	0.27	10.1	2.68

Table 11: Summary of the maximum value of the horizontal displacement calculation.

Work conditions	Horizontal displacement (m)
Construction period 12 months	0.420
Construction period 18 months	0.402
Construction period 24 months	0.391

in the foundation, and its maximum value occurs in the section between the edge of the rockery and the highest place of the mound construction, near the elevation range of 417–420 m. The direction is away from the rockery, its maximum value occurs at the end of construction, and the horizontal displacement generated by the consolidation at the end of construction is minimal and negligible. The maximum values of the calculated horizontal displacements are summarized in Table 11.

3.4. Jingshan Mountain Resistance Stability Analysis

3.4.1. Calculated Working Conditions (Considering Overhole Pressure). Assuming the working condition of superporous pressure is considered, the effective stress method is used to calculate the anti-slip stability of the slope of the Jingshan Mountain project in Meibei Lake scenic area, and the superporous pressures of the foundation and the rockery are determined based on the superporous pressure field obtained from the consolidation calculation.

The calculation times are the end of construction, 12 months and 24 months after the end of construction, respectively. The same division of the construction period is 12 months, 18 months, and 24 months.

3.4.2. Calculation Process (Considering Overhole Pressure). Due to the complexity of the calculation process, the detailed calculations are not included in this section. However, for the construction period of 24 months, the results of slip resistance stability calculations at the end of construction, 12 months after the end of construction, and 24 months after the end of construction are presented in Figure 13.

3.4.3. Analysis of Calculation Results (Considering Overhole Pressure). This section presents the calculation results (Table 12) for profile 3-3 with a small slip resistance stability coefficient. The results show that the selected profile has a slip stability coefficient minimum value of 2.24 during the construction period and the subsequent consolidation process (24 months) and of 1.72 considering the seismic effect (seismic acceleration 0.2 g), which satisfies the slip stability requirement.

The stability calculation results show that the superporous pressure in the foundation gradually dissipates with the consolidation of the foundation at the end of construction, and the anti-slip stability coefficient gradually increases, but the magnitude is not large.

Moreover, the longer the assumed construction period is, the smaller the superporous pressure formed in the foundation, and the anti-slip stability coefficients of the profile will all be improved.

3.4.4. Calculated Working Conditions (without Considering Overhole Pressure). Assuming that the working condition of superporous pressure is not considered, the area comprises a seismic intensity zone of 8°, and the calculation working condition is calculated according to the two cases of normal operation and special operation using Autobank 7.7 software of Riverhead University, and the landslide stability of the mountain is calculated using the Swedish arc method and Bishop's method.

3.4.5. Calculation Process (without Considering the Overhole Pressure). Eight profiles were selected for the calculation, and due to the complexity of the process, it is not listed in this section. The results of the anti-slip stability calculation are presented in Figure 14. Profile 3-3 is shown as an example to illustrate the findings.

3.4.6. Analysis of Calculation Results (without Considering Overhole Pressure). When not considering the overhole pressure, the stability calculation results for each profile are as shown in Table 13.

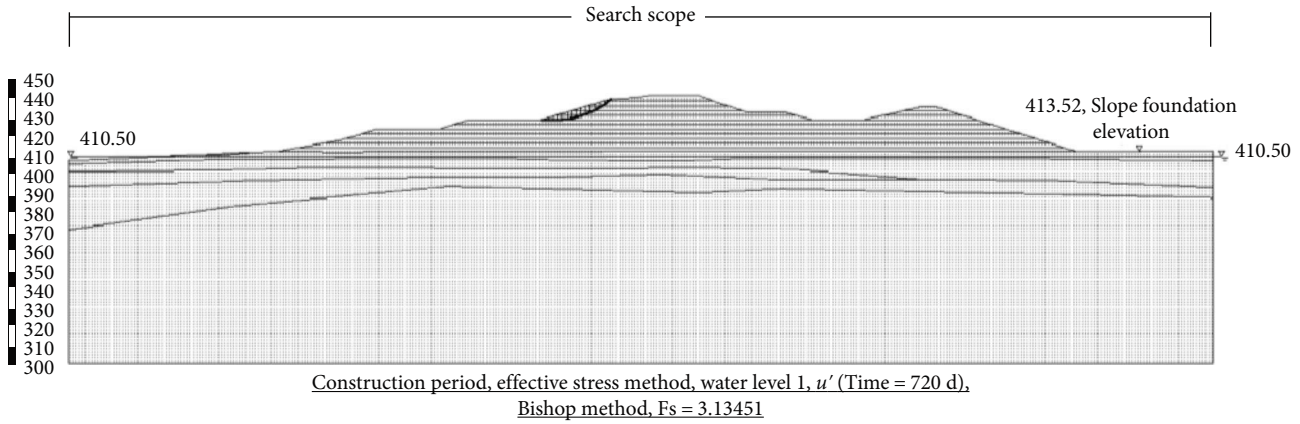

Construction period, effective stress method, water level 1, u' (Time = 720 d),
Bishop method, Fs = 3.13451

(a)

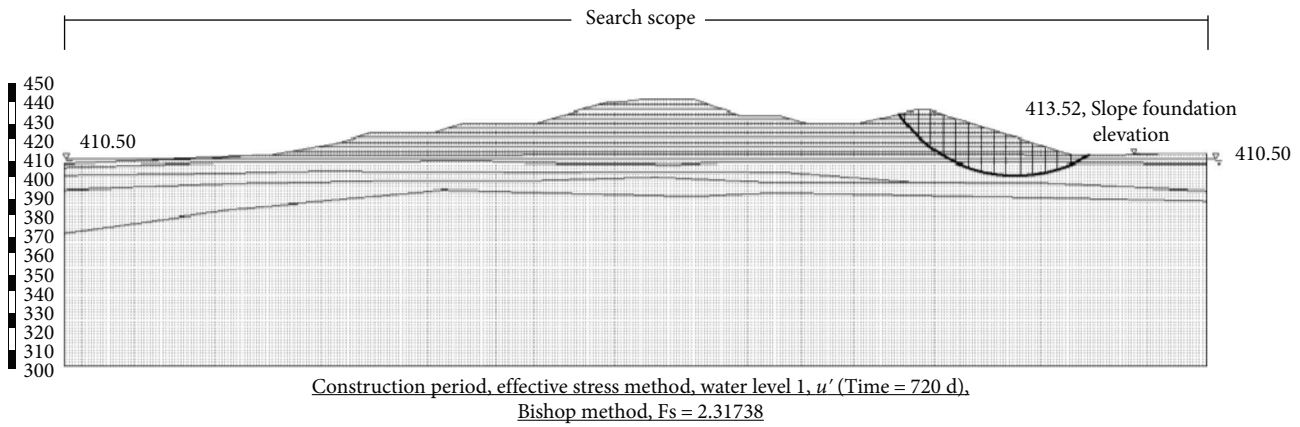

Construction period, effective stress method, water level 1, u' (Time = 720 d),
Bishop method, Fs = 2.31738

(b)

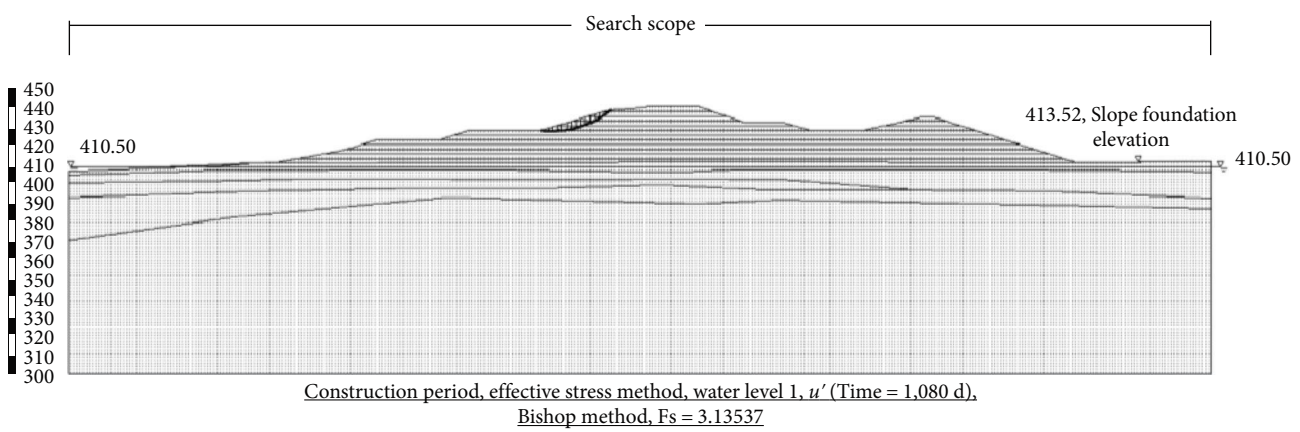

Construction period, effective stress method, water level 1, u' (Time = 1,080 d),
Bishop method, Fs = 3.13537

(c)

Figure 13: Continued.

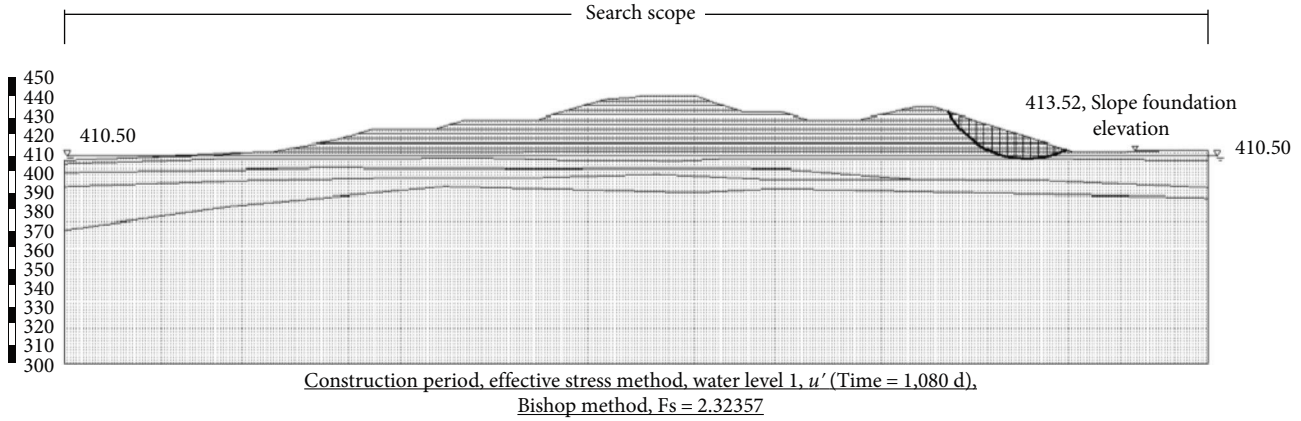

(d)

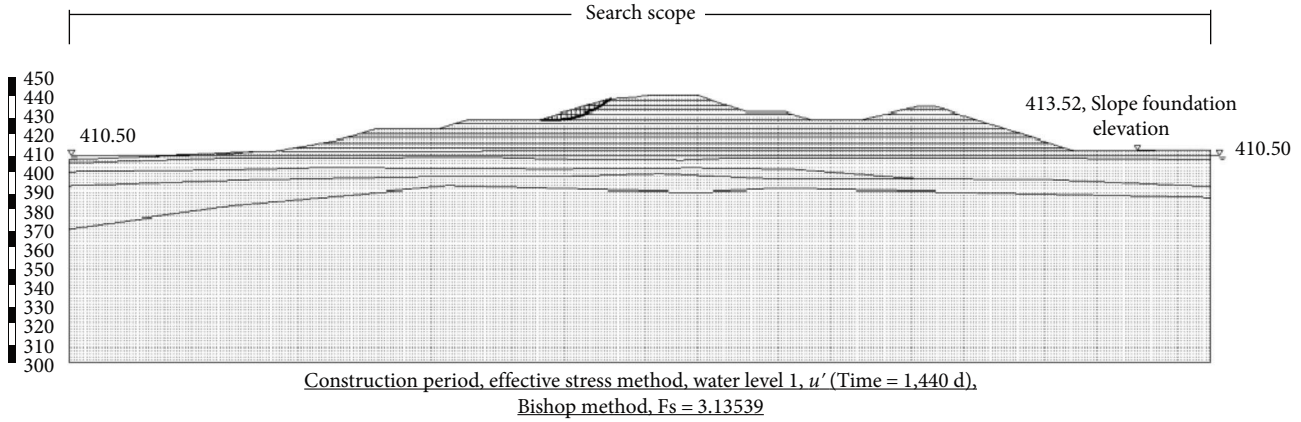

(e)

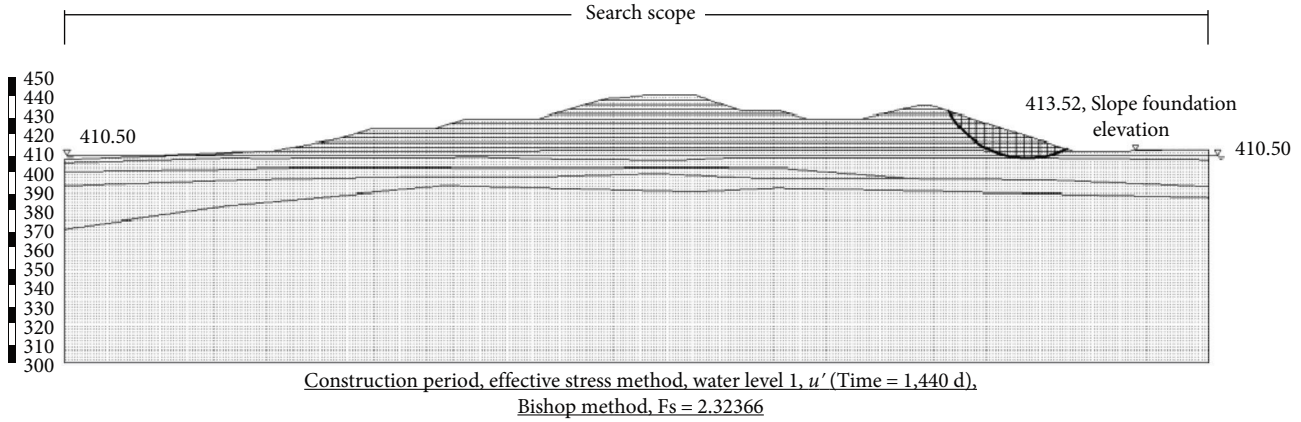

(f)

Figure 13: Slip resistance stability calculation results. (a) After construction (sliding to the left). (b) After construction (sliding to the right). (c) Twelve months after the end of construction (sliding to the left). (d) Twelve months after the end of construction (sliding to the right). (e) Twenty-four months after the end of construction (sliding to the left). (f) Twenty-four months after the end of construction (sliding to the right).

The minimum safety factor of the Swedish method is 1.463 for normal conditions and 1.167 for earthquake conditions, and the minimum safety factor of the Bishop method is 1.598 for normal conditions and 1.268 for earthquake conditions, meeting the requirements of the relevant codes.

4. Recommendations

4.1. Foundation Settlement and Deformation Reduction in Mountain-Mounding Construction. The core problem of the mountain-mounding project is how to mitigate

Table 12: Summary of slip stability coefficients for Profile 3-3.

Profile 3-3	Calculated working conditions	End of construction	End of 12 months	End of 24 months
Filling period 12 months slip resistance stability factor	Sliding to the left	3.13346	3.13532	3.13539
	Sliding to the right	2.18455	2.24773	2.24786
	Left + earthquake	2.28345	2.28486	2.28492
	Right + earthquake	1.72585	1.79245	1.79256
Filling period 18 months slip resistance stability factor	Sliding to the left	3.13415	3.13535	3.13539
	Sliding to the right	2.26386	2.26834	2.26845
	Left + earthquake	2.28397	2.28489	2.28492
	Right + earthquake	1.80197	1.80216	1.80225
Filling period 24 months slip resistance stability factor	Sliding to the left	3.13451	3.13537	3.13539
	Sliding to the right	2.31738	2.32357	2.32366
	Left + earthquake	2.28425	2.2849	2.28492
	Right + earthquake	1.83627	1.84516	1.84523

foundation settlement deformation during construction and long-term use. The project involves a tall mountain with a significant self-weight stress. The central part of the mountain is subjected to a calculated load of up to 500 kPa, and the underlying main bearing layer consists of soft plastic state ②-2 loess-like soil (Q4al + pl). Two key engineering geological issues arise: uneven settlement deformation in the vertical direction, which can lead to cracks in the mountain, and foundation shear damage due to the mound load exceeding the soil's strength. Therefore, it is crucial to consider scientifically and reasonably engineered techniques throughout the construction process to address these challenges effectively.

Effective measures should be taken to avoid the problems of large consolidation deformation and uneven settlement even after the completion of the mountain. First, since the mound is high in the middle and low around, the load is uneven, so the corresponding foundation should be drained and reinforced in advance according to the different load sizes; Second, the ground settlement caused by the compressive deformation of the mountain during the process of mounding is large and requires a considerable amount of time to stabilize. To mitigate foundation settlement during the construction, the speed of filling mounding and the loading time should both be controlled. Third, during the construction of the mounded mountain, the height of the filling should be reserved according to the settlement rate and the elevation of the top of the mountain to ensure the overall beauty of the scenic mountain.

Some previous experience shows that where the amount of subsidence is less than 1% of the mountain height, cracks will generally not be produced, and the amount of subsidence is greater than 3% of the mountain height of most of the cracks. If cracks are not produced within 2–3 years after the completion of the mountain-mounding, cracks will generally not be produced thereafter.

4.2. Enhanced Drainage and Controlled Construction and Monitoring for Improved Stability. To expedite the drainage consolidation time of the foundation under load, a material with good permeability should be laid on its surface to shorten the drainage path so that the pore water pressure in the soil can be fully dissipated and the shear strength of the soil can be improved. This will also be beneficial for accurately controlling the construction loading rate. During construction, the quality of the filling and the number of rolling should be strictly controlled, and the construction should be carried out strictly according to the design to reduce the deformation of the mountain itself. In addition, under the condition that the construction period allows, a reasonable profile form, loading increment, and rate should be adopted to ensure the overall stability and the deformation stability. On-site monitoring, including lateral displacement and settlement monitoring, should be carried out throughout the construction process, and a dense combination of dynamic monitoring results should be used to form a complete information construction system.

4.3. Impact of These Measures on the Surrounding Buildings (Structures). The foundation settlement, and ground uplift caused by mountain-mounding construction project will inevitably have an impact on the surrounding residential buildings, roads, pipelines, and the other municipal public buildings. However, by taking the above effective measures, the impact can be reduced or even eliminated to a certain extent. The site and the nearby buildings and facilities should be also thoroughly investigated before construction, and the damage impact of the above facilities should be strictly monitored during construction to prevent safety accidents.

4.4. Slope Reinforcement for Waste Mountain-Mounding Construction. The final displacement of the mountain can reach an impressive 2.0 m after 720 days, indicating a significant magnitude of movement. Therefore, it is highly necessary to reinforce the mountain using anchor rods. Anchor rod structures serve as effective reinforcement methods for slope support, effectively preventing water infiltration in loess slopes and reducing the potential for soil saturation-induced slope failure. By employing a rational design of retaining wall structures, in conjunction with anchor rods, a composite system is formed that facilitates force distribution and coordination. This composite system not only improves the mechanical properties of the soil but also enhances its overall strength (Figure 15).

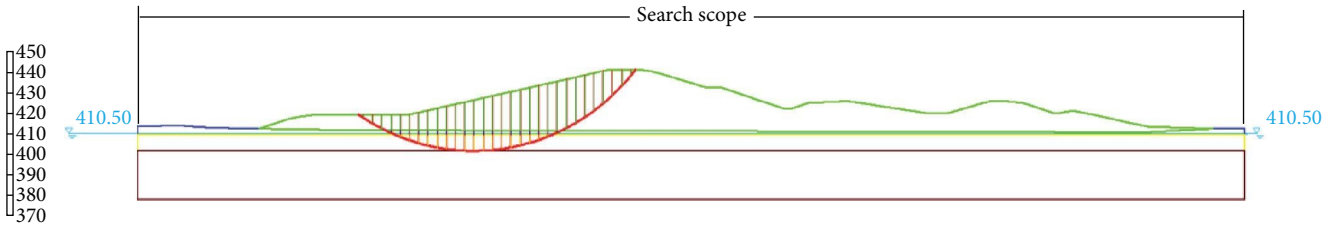

Normal operation period, total stress method, water level 1, Bishop method, Fs = 2.56505

(a)

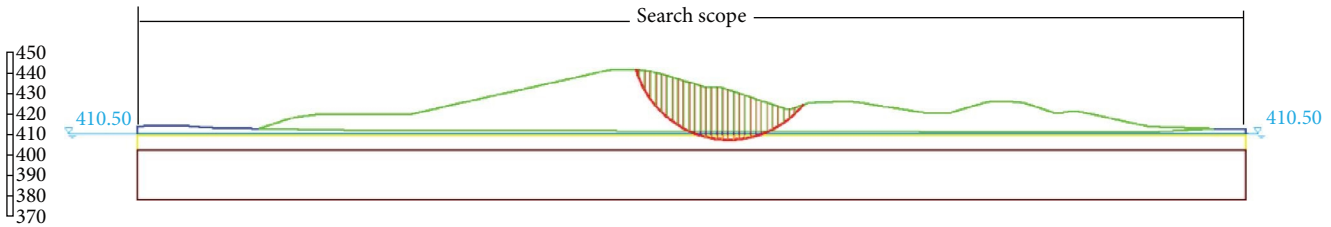

Normal operation period, total stress method, water level 1, Swedish method, Fs = 2.36315

(b)

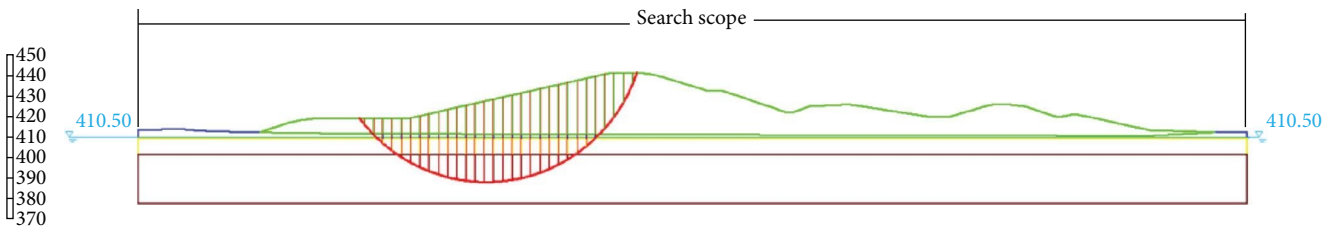

Normal operation period, total stress method, water level 1, Swedish method, Fs = 2.27399

(c)

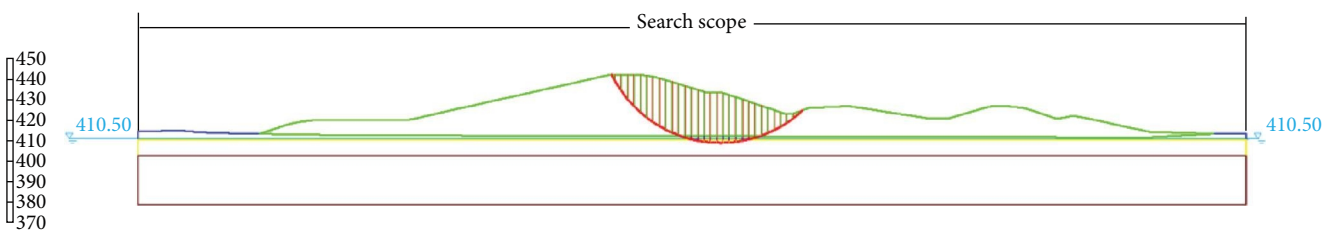

Normal operation period, total stress method, water level 1, Bishop method, Fs = 2.69717

(d)

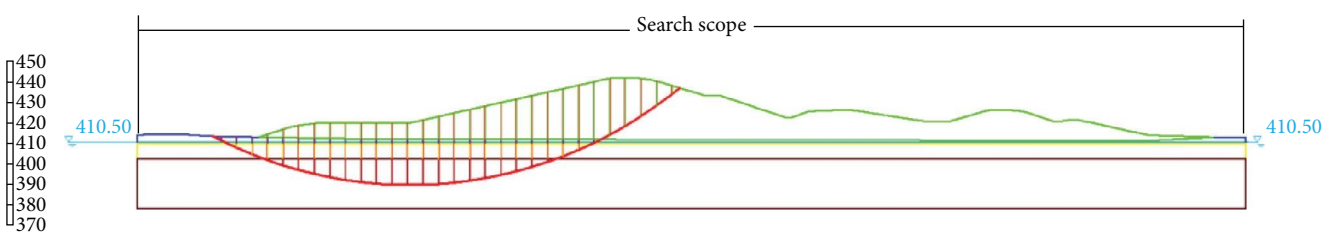

Normal operation period, total stress method, water level 1, Bishop method, 0.2 g, Fs = 1.82177

(e)

Figure 14: Continued.

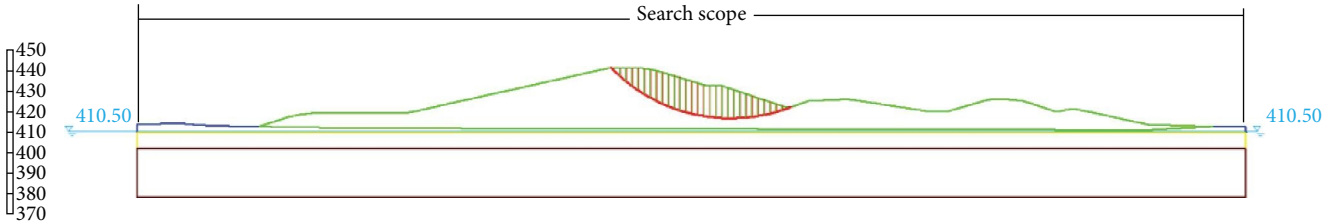

(f)

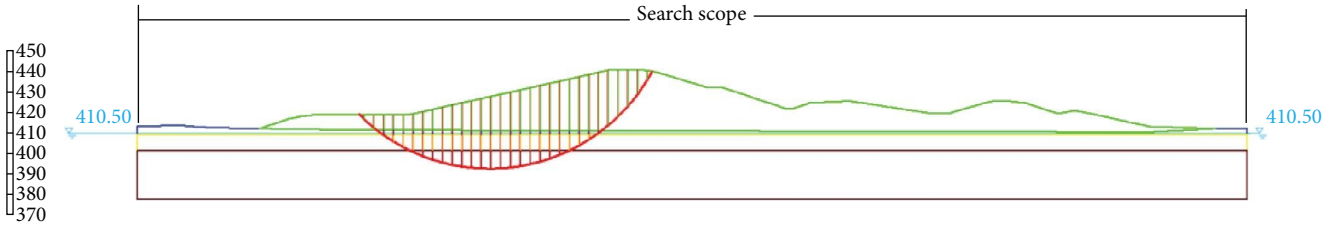

(g)

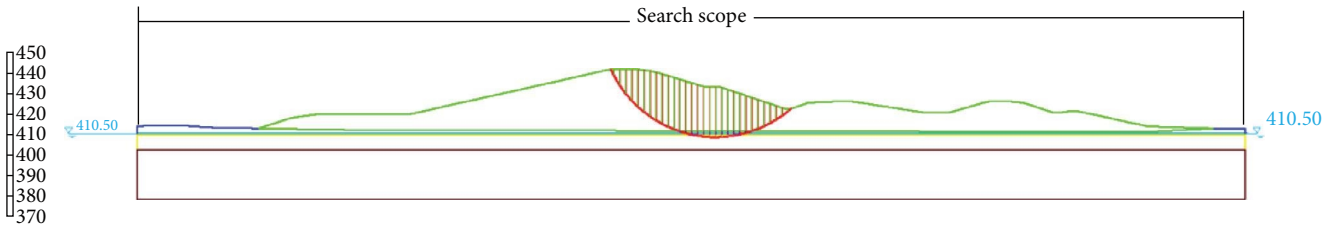

(h)

Figure 14: Slip resistance stability calculation results. (a) Normal working condition of profile 3-3: Bishop method of anti-slip stability calculation slip arc position (normal sliding to the left). (b) Normal working condition of profile 3-3: Bishop method slip stability calculation slip arc position (normal sliding to the right). (c) Normal working condition of profile 3-3: Swedish method of anti-slip stability calculation slip arc position (normal sliding to the left). (d) Normal working condition of profile 3-3: Swedish method of anti-slip stability calculation slip arc position (normal sliding to the right). (e) Seismic condition of profile 3-3: Bishop method slip stability calculation slip arc position (normal sliding to the left). (f) Seismic condition of profile 3-3: Bishop method slip stability calculation slip arc position (normal sliding to the right). (g) Seismic condition of profile 3-3: Swedish method of anti-slip stability calculation slip arc position (normal sliding to the left). (h) Seismic condition of profile 3-3: Swedish method of anti-slip stability calculation slip arc position (normal sliding to the right).

Table 13: Summary of stability calculations for each profile.

Profile	Normal working condition				Seismic conditions			
	Bishop		Sweden		Bishop		Sweden	
	Left	Right	Left	Right	Left	Right	Left	Right
1-1	1.598	1.929	1.470	1.768	1.279	1.474	1.170	1.340
2-2	2.565	2.697	2.274	2.363	1.822	1.991	1.643	1.752
3-3	2.737	1.740	2.506	1.624	1.750	1.405	1.650	1.299
4-4	2.077	2.039	1.892	1.818	1.647	1.609	1.516	1.430
5-5	2.321	1.893	2.116	1.748	1.809	1.473	1.674	1.355
6-6	1.953	2.593	1.778	2.349	1.469	1.724	1.333	1.578
7-7	1.638	1.736	1.492	1.591	1.268	1.337	1.177	1.217
8-8	1.637	1.779	1.463	1.634	1.281	1.369	1.167	1.252

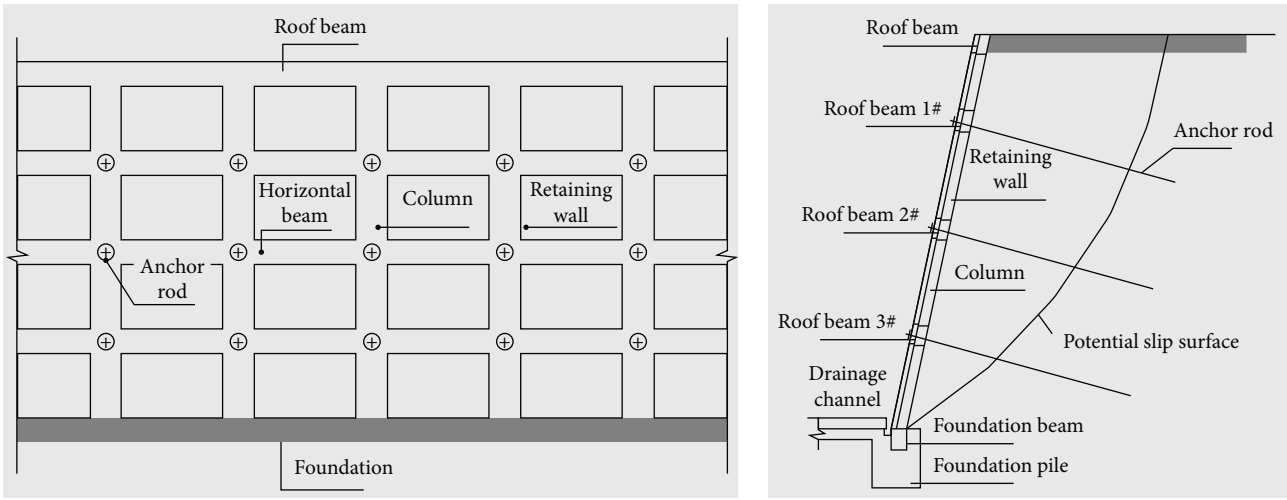

Figure 15: Elevation and sectional view of the support structure.

5. Conclusions

(1) During construction, the overall settlement rate increases initially, then decreases gradually. Settlement increases with added fill material and load, but stabilizes after filling is complete. When constructing artificial Jing Shan, implementing sound material quality, construction plan selection, and process control can effectively address high-embankment deformation.

(2) Steep slopes and fast loading rates can undermine slope stability. Properly designed slope angles, controlled loading rates, and adjusted construction planning effectively address high-embankment slope stability.

(3) To mitigate soil erosion during construction, the Jing Shan project should harmonize the surface drainage system with the natural water collection features of the surroundings, preventing excessive hillside erosion from rainfall.

Data Availability

All data used to support the study are included within the article.

Conflicts of Interest

The authors declare that they have no conflicts of interest.

Authors' Contributions

Miao Kang, Xiongbin Guo, and Shoufu Li proposed the idea. All authors contributed to the material sourcing. Teng Wang, Weiye Gu, and Yufei Xu conducted the experiments. Jincheng Fan performed the data analysis. Yufei Xu and Jincheng Fan discussed the results and contributed to the final manuscript.

Acknowledgments

This paper is sponsored by Scientific research Project of China Construction Third Engineering Bureau Group Co., Ltd. (Program No. CSCEC3B-2020-5).

References

[1] L. Zhang, K. Fu, S. M. Zhang, L. Zhong, and L. Wang, "Study on stability analysis and engineering protection measures of construction waste dump," *Tianjin Science and Technology*, vol. 48, no. 5, pp. 80–83+87, 2021.

[2] G. Y. Fu, "Application of construction waste in the city park," *Brick-Tile*, vol. 4, pp. 42-43, 2013.

[3] Y. Chen, L. Tan, N. Xiao, K. Liu, P. Jia, and W. Zhang, "The hydro-mechanical characteristics and micro-structure of loess enhanced by microbially induced carbonate precipitation," *Geomechanics for Energy and the Environment*, vol. 34, Article ID 100469, 2023.

[4] X. J. Liu, H. Q. Li, H. Y. Lei, P. Wang, and C. Q. Qi, "Application of large-scale software ANSYS to piling mountain project," *Rock and Soil Mechanics*, vol. S2, pp. 357–360, 2004.

[5] J. Han, J. Wang, D. Jia et al., "Construction technologies and mechanical effects of the pipe-jacking crossing anchor-cable group in soft stratum," *Frontiers in Earth Science*, vol. 10, Article ID 1019801, 2023.

[6] J. Han, J. Wang, C. Cheng et al., "Mechanical response and parametric analysis of a deep excavation structure overlying an existing subway station: a case study of the Beijing subway station expansion," *Frontiers in Earth Science*, vol. 10, Article ID 1079837, 2023.

[7] H. Y. Lei, H. Q. Li, X. J. Liu, Z. Y. Zhang, and Z. R. Wan, "Discussion on stability evaluation of soft soil foundations beneath artificial hills," *Rock and Soil Mechanics*, vol. S2, pp. 589–593, 2004.

[8] F. Ma, H. Y. Lei, Y. M. Ying, and J. W. Bai, "Monitoring and control of foundation stability of a construction site on waste disposal area in Tianjin City," *The Chinese Journal of Geological Hazard and Control*, vol. 3, pp. 124–126+132, 2006.

[9] J. J. Cang, Y. F. Guan, H. H. Chen, and J. C. Liu, "Numerical analysis for foundation treatment and stability of muddy soil during artificially piling mountain in soft soil areas," *Journal of Water Resources and Architectural Engineering*, vol. 10, no. 1, pp. 31–35, 2012.

[10] Z. R. Wan, H. Y. Lei, and H. J. Liu, "Application of reverse analysis method for displacement to stability of construction waste landfiil site," *Environmental Sanitation Engineering*, vol. 13, no. 4, pp. 1–3, 2005.

[11] H.-Y. Lei, H.-B. Lu, and J.-W. Bai, "Design and construction of a piled mountain with engineered municipal construction waste over soft clay," *Geotechnical and Geological Engineering*, vol. 35, no. 4, pp. 1341–1356, 2017.
[12] C. Q. Qi, "Research on piled mountain landscape on construction waste landfill site in Tianjin," *Environmental Sanitation Engineering*, vol. 10, no. 3, pp. 113–115, 2002.
[13] F. Chen, X. Li, Y. Yang, H. Hou, G.-J. Liu, and S. Zhang, "Storing E-waste in green infrastructure to reduce perceived value loss through landfill siting and landscaping: a case study in Nanjing, China," *Sustainability*, vol. 11, no. 7, Article ID 1829, 2019.
[14] J. J. Li, *Stability Evaluation of Soil Foundations Beneath Artificial Hills in Tianjin*, China University of Geosciences Beijing, 2007.
[15] Y. Miao and H. B. Chen, "Application of numerical simulation of triaxial tests on stability analysis of construction waste slope based on PFC3D," *Environment and Sustainable Development*, vol. 42, no. 3, pp. 74–77, 2017.
[16] Z. M. Kang and L. L. Li, "Analysis on current treatment and resource utilization of construction waste in Xi'an," *Northwest Hydropower*, vol. S2, pp. 91–95, 2020.
[17] H. N. Wang, *Research of Xi'an Construction Waste Resource Utilization*, Chang'an University, 2014.
[18] Z. Y. Tang, *A Study on Resource Recycle of Construction Waste in Xi'an*, Chang'an University, 2017.
[19] M. K. Ma, *Research on the Multiple Cooperative Governance of Urban Construction Waste Recycling—A Case Study of Xi'an City*, Chang'an University, 2019.
[20] L. J. Zhang, "Research on reuse of construction waste residue in Xi'an," *Environmental Engineering*, vol. 35, no. 5, pp. 122–124, 2017.